The Journal of Neuroscience, November 1, 1997, 17(21):8427–8442

Synaptic Communication among Hippocampal Interneurons: Properties of Spontaneous IPSCs in Morphologically Identified Cells

Norbert Hájos and Istvan Mody

Departments of Neurology and Physiology, Reed Neurological Research Center, University of California, Los Angeles, School of Medicine, Los Angeles, California 90095-1769

The properties of spontaneous IPSCs (sIPSCs) recorded with whole-cell patch-clamp techniques were investigated in various anatomically identified hippocampal CA1 interneurons and were compared with those recorded in pyramidal cells. Neurons labeled with biocytin or neurobiotin were classified on the basis of their dendritic and axonal arborizations, leading to the identification of previously unknown interneuron types projecting to the dendritic region of pyramidal cells. In most interneurons, the average sIPSCs decayed slower than did those observed in pyramidal cells. The properties of sIPSCs were homogeneous within a given morphologically identified neuron type. Many interneurons had comparable somatic size, location, and dendritic arbor but displayed extremely different axonal projections paralleled by distinct sIPSC properties. Thus, physiological comparisons are only meaningful after the complete morphological identification of the recorded cells. The decay of sIPSCs matched for amplitudes and rise times could vary over 10-fold in a given interneuron, consistent with electrotonic filtering and possibly with different $GABA_A$ receptor subunit assemblies present at distinct synapses. Our findings demonstrate an extensive connectivity among hippocampal interneurons through $GABA_A$ synapses of various properties that may underlie complex network oscillations at different frequencies.

Key words: hippocampus; nonpyramidal cells; intracellular labeling; inhibition; network; oscillation; GABA; $GABA_A$ receptors

The anatomical, physiological, and biochemical characterization of different types of hippocampal interneurons has expanded considerably (for review, see Freund and Buzsáki, 1996). Intracellular labeling studies have begun to classify interneurons according to the spatial selectivity of their axonal and dendritic trees (Gulyás et al., 1993; Han et al., 1993; Buhl et al., 1994; Buckmaster and Schwartzkroin, 1995; Sik et al., 1995). These studies have defined two main groups of interneuron, the perisomatic and the dendritic inhibitory cells, each likely controlling distinct aspects of postsynaptic electrogenesis by innervating specific spatial domains of principal cells (Miles et al., 1996). Perisomatic interneurons, including the axo-axonic and basket cells, are less multiform than are dendritic inhibitory cells such as the O-LM, HIPP, bistratified, or horizontal trilaminar cells that show a high variety in their input and output characteristics (Han et al., 1993; Buhl et al., 1994; McBain et al., 1994; Sik et al., 1995).

As we learn more and more about interneurons, the classical view about their purely inhibitory function is also changing. Interneurons are now thought to provide the necessary timing mechanism for both low and high frequency firing of principal cells (Soltesz and Deschênes, 1993; Bragin et al., 1995; Buzsáki and Chrobak, 1995; Cobb et al., 1995; Whittington et al., 1995; Jefferys et al., 1996). Connected interneuronal networks can sustain gamma oscillations (20–70 Hz) without any requirement for fast excitatory synaptic drive (Whittington et al., 1995; Traub et al., 1996) and, by sustaining such oscillations, may participate in higher cognitive functions (Singer, 1993; Gray, 1994). Various modeling studies (Traub et al., 1996; Wang and Buzsáki, 1996) have suggested that the frequency for such network oscillations is critically dependent on the kinetic properties of $GABA_A$ receptor-mediated events in interneurons and on the nature of the connectivity among them. A specific control of interneuronal networks may originate from a recently identified new class of hippocampal interneuron specialized to innervate only other interneurons (Acsády et al., 1996b; Gulyás et al., 1996; Hájos et al., 1996).

To better understand the operation of the interneuronal network, it is important to determine the specific properties of $GABA_A$ receptor-mediated synaptic currents in different interneurons. To date, the properties of spontaneous IPSPs and IPSCs (sIPSCs) have been examined mainly in principal cells of the hippocampus, neocortex, and cerebellum (Otis and Mody, 1992; Vincent et al., 1992; Puia et al., 1994; Salin and Prince, 1996). The only GABAergic interneuron examined so far for its sIPSCs is the cerebellar stellate cell in which IPSCs with rapid rise and slow decay could be recorded (Llano and Gerschenfeld, 1993). Such data are not available for morphologically identified hippocampal interneurons. Some previous studies have examined the inhibition in interneurons using sharp microelectrodes or have recorded evoked IPSCs (Misgeld and Frotscher, 1986; Lacaille et al., 1987; Lacaille and Schwartzkroin, 1988a,b; Lacaille, 1991; Williams et al., 1994; Morin et al., 1996). These studies, however, lacked proper morphological identification of the recorded cells and may have failed to achieve the high resolution afforded by patch-clamp techniques that is necessary to reveal small amplitude synaptic

Received April 21, 1997; revised Aug. 12, 1997; accepted Aug. 15, 1997.

This work was supported by National Institutes of Health Grants NS 27528 and NS 30549 to I.M. N.H. was also supported by OTKA (F17115). We thank Drs. T. F. Freund and S. R. Williams for critical comments on this manuscript, Dr. C. R. Houser for allowing us to use the camera lucida, and Brian K. Oyama and Michael T. Kim for excellent technical assistance.

Correspondence should be addressed to Dr. Istvan Mody, Departments of Neurology and Physiology, Reed Neurological Research Center, University of California Los Angeles School of Medicine, 710 Westwood Plaza, Los Angeles, CA 90095-1769.

activity (Soltesz and Mody, 1994). In the present study we recorded $GABA_A$ receptor-mediated spontaneous IPSCs in hippocampal interneurons of the CA1 region using the whole-cell patch-clamp technique. We filled each cell with biocytin or neurobiotin and reconstructed their axonal and dendritic arbors, allowing a complete anatomical identification. The synaptic communication among hippocampal interneurons shows a large heterogeneity of sIPSC kinetics that most likely results from the presence of different $GABA_A$ receptor subunit assemblies at distinct synapses.

MATERIALS AND METHODS

Slice preparation. Young (20–28 d old) male Wistar rats were decapitated under deep sodium pentobarbital anesthesia (70 mg/kg, i.p.). After the skull was opened, the head was immersed in cold (~4°C), modified artificial CSF (ACSF), and the brain was removed. This ACSF contained (in mM): 126 NaCl, 2.5 KCl, 26 $NaHCO_3$, 0.5 $CaCl_2$, 10 $MgCl_2$, 1.25 NaH_2PO_4, 10 glucose, and 2 kynurenic acid (Sigma, St. Louis, MO). Coronal slices (350–450 μm thick) were prepared using a Lancer Series 1000 Vibratome. The slices were sagittally bisected along the midline and were incubated in a storage chamber in ACSF (containing $CaCl_2$ and $MgCl_2$ at 2 mM) for 30 min at 32°C, and then the whole chamber was transferred to room temperature (22–23°C). For the preparation of longitudinal slices, the whole brain was sagittally cut into two halves, and the hemispheres were glued on their callosal side onto a slope of 45° before slicing with the Vibratome. Longitudinal sagittal slices (400 μm thick) were cut parallel to the axis of the hippocampus.

Whole-cell recordings. Whole-cell voltage-clamp recordings were obtained from interneurons and pyramidal cells visualized by infrared DIC (IR–DIC) (Axioscope; Zeiss) videomicroscopy (Sakmann and Stuart, 1995). Patch electrodes were pulled from borosilicate glass capillaries with inner filament (KG-33, 1.5 mm outer diameter; Garner Glass) using a two-stage vertical Narishige PP-83 puller and had a resistances of 2–6 MΩ. The intrapipette solution was prepared from Omnisolve water (EM Science, Gibbstown, NJ) and contained (in mM): 135 Cs gluconate, 5 CsCl, 20 HEPES, 2 $MgCl_2$, 2 Mg-ATP, and 1–1.5% biocytin (Sigma, St. Louis, MO) or neurobiotin (Vector Laboratories, Burlingame, CA) at pH 7.2–7.3, adjusted with CsOH yielding an approximate Cl^- reversal potential ($E_{Cl}-$) of −45 mV. Final osmolarity was 290–310 mOsm.

During experiments, slices were superfused continuously with oxygenated (95 %O_2/5% CO_2) ACSF containing 2 mM kynurenic acid to block fast ionotropic glutamate receptors. All experiments were performed at room temperature (22–23°C) within 6.5 hr of slicing. Neurons were mainly sampled in coronal slices unless indicated otherwise. Recordings were made with an Axopatch 2A or B amplifier (Axon Instruments), digitized at 88 kHz (Neurocorder; NeuroData), and stored on videotape. Off-line, the data were filtered at 1–1.5 kHz (eight pole Bessel; Frequency Devices 9002), digitized at 5–10 kHz (National Instruments Lab PC+ analog-to-digital board), and analyzed using the Strathclyde Electrophysiology Software (courtesy of Dr. J. Dempster). The series resistances were constant (±10%) during the period of analysis of sIPSCs (2–5 min) and are indicated for each neuron in Table 1. The liquid junction potential was reduced using an agar bridge (Neher, 1992). Events were detected as described in detail elsewhere (Otis and Mody, 1992). The distributions of amplitudes, 10–90% rise times, and half decay times (T50%, i.e., the time required for an IPSC to decay to 50% of its peak amplitude) of sIPSCs are plotted as cumulative probabilities drawn on a probability scale ordinate (Origin 4.1; Microcal). In all cases, the average sIPSCs were obtained from the most frequent 60% of all events, i.e., from those IPSCs falling between 20 and 80% of the cumulative probability distributions of amplitudes. The sIPSC time course was determined by fitting single or average events using a least-squares Simplex-based algorithm with the sum of two (one rising and one decaying) or three (one rising and two decaying) exponentials (Soltesz and Mody, 1995) of the form:

$$I(t) = -A \cdot e^{-\tau_R/t} + A_1 \cdot e^{-\tau_{D1}/t} + A_2 \cdot e^{-\tau_{D2}/t}, \quad (1)$$

where $I(t)$ is the sIPSC as a function of time; $A_1 + A_2 = A$ are constants; and τ_R, τ_{D1}, and τ_{D2} are the rise, fast decay, and slow decay time constants, respectively. For single exponential decays, A_2 was set to zero. To evaluate the improvement of the fit by adding a second exponential decay component, we used an F test as described in detail elsewhere (Soltesz and Mody, 1995). The Kolmogorov–Smirnov (K–S) statistical test was used to compare two different cumulative distributions using SPSS for Windows. We have chosen a significance level of 10^{-4} for the K–S statistic. Data are presented as mean ± SE (n = number of cells).

Anatomical identification of interneurons. At the end of the recordings, slices were placed back into the storage chamber for 1 hr and then fixed overnight in 4% paraformaldehyde, 0.05% glutaraldehyde, and 15% picric acid in 0.1 M phosphate buffer (PB), pH 7.4. The slices were resectioned at 80 μm with the Vibratome, incubated in cryoprotecting solution (0.01 M PB containing 12% glycerol and 25% sucrose) for 30 min, freeze-thawed three times above liquid nitrogen, and treated with 0.5% H_2O_2 in 0.1 M PB for 30 min to reduce endogenous peroxidase activity. Injected neurons were visualized using avidin-biotinylated horseradish peroxidase complex reaction (ABC; Vector Laboratories, Burlingame, CA) with nickel-intensified 3,3′-diaminobenzidine (Sigma, St. Louis, MO) as chromogen (dark blue reaction product). After dehydration and embedding in Durcupan, the representative neurons were reconstructed with the aid of a drawing tube at 40–100× magnification. The lengths of the dendrites were measured using the National Institutes of Health image program after digitization with a CCD camera.

Reagents. Bicuculline (Sigma, St. Louis, MO) was applied by bath perfusion in final concentrations of 30 μM. All other salts and reagents were obtained from Fluka.

RESULTS

In the presence of the ionotropic glutamate receptor antagonist kynurenic acid (2 mM), the frequencies of the sIPSCs varied between 0.5 and 6.4 Hz in interneurons and 1.2 and 10 Hz in pyramidal cells (Table 1). The sIPSCs were outward at a holding potential of 0 ± 5 mV, were reversed at E_{Cl^-} (near −45 mV), and were blocked by the $GABA_A$ receptor antagonist bicuculline (30 μM; n = 4; data not shown).

Recordings were obtained from a total of 72 interneurons and 5 pyramidal cells. After visualization of biocytin or neurobiotin, the neurons were classified according to their morphology. Only 36% (n = 28) of the cells were included in the detailed analysis of sIPSC properties. In these cells, the morphology could be properly described, i.e., the neurons had well-stained dendritic *and* axonal arbors. The interneurons excluded from our study could not be completely reconstructed either because of their proximity to the slice surface or because of the incomplete labeling.

Differences in sIPSC properties between pyramidal cells and interneurons

The amplitudes of sIPSCs recorded in pyramidal cells (Fig. 1*A*) were larger than those found in interneurons (Fig. 1*D*,*F*), but the distributions of the rise times were similar (Fig. 1*F*). In general, the half decay times (T50%) were also different (see the comparison of pyramidal cells and an O-LM cell in Fig. 1*E*,*F*), but some interneurons, e.g., radial trilaminar cells, had sIPSC T50% similar to those recorded in pyramidal cells (Table 1). In three anatomically identified pyramidal cells, the average sIPSC properties were homogeneous (Fig. 1*D*). The mean amplitude and fast rise-time constant of the averages were 34.3 ± 2.7 pA and 0.49 ± 0.05 msec, respectively (n = 3). Furthermore, the cumulative distributions of sIPSC amplitudes, rise times, and T50% were also well matched between pyramidal cells (Fig. 1*F*; Table 1). A recording in a longitudinal slice from a neuron with pyramidal cell-like morphology in the stratum (str.) radiatum, spiny dendrites located in strata radiatum and lacunosum-moleculare, and its axon projecting to str. oriens (Maccaferri and McBain, 1996) revealed sIPSC kinetics similar to those found in pyramidal cells (Table 1) but with a smaller average amplitude (20.7 pA).

Table 1. sIPSC properties in morphologically identified hippocampal CA1 neurons

Cell types	Code #	*Rs* MΩ	sIPSC frequency (Hz)	Average amplitude (pA)[a]	τ_R of average (msec)	Median T50% (msec)	10–90% Range of T50% (msec)
O-LM cells in coronal slices, Fig. 1*C*	H0416	10.6	1.4	17.3	0.38	8.2	2.1–16.8
	H0630	15.5	1.7	22.0	0.65	8.7	3.1–16.2
	H0749	13.6	1.3	12.2	0.44	11.1	3.7–22.1
	H0754	11.7	1.6	17.6	0.38	11.2	4.5–18.9
	H0756	10.0	1.5	16.1	0.35	9.6	1.9–18.9
O-LM cells in longitud. slices	H0763	10.1	5.3	19.3	0.37	7.2	2.8–13.5
	H0946	14.3	2.9	14.6	0.49	7.0	2.5–13.2
Bistartified cell, Fig. 6*A*	H0759	8.6	1.2	19.0	0.30	8.1	1.5–15.9
Radial trilaminar cells as in Fig. 5*A*	H0741	10.6	3.1	22.0	0.31	9.7	4.9–12.6
	H0742	11.0	0.8	18.9	0.59	9.3	5.1–11.1
Radial trilaminar cells as in Fig. 5*B*	H0405	11.6	3.3	21.3	0.32	7.2	1.3–14.8
	H0414	11.7	0.5	19.5	0.31	9.4	2.1–13.3
	H0634	8.6	3.1	36.7	0.51	8.7	2.5–11.4
Multipolar cells projecting to strata radiatum and lacusosum-moleculare as in Fig. 7*B*[b]	H0413	10.1	0.7	16.8	0.35	6.0	1.3–11.4
	H0619	8.3	6.4	31.3	0.51	6.4	2.1–13.2
	H0628	11.9	1.8	22.8	0.45	7.0	2.1–14.4
Str. radiatum cells as in Fig. 7*A*	H0352	15.4	3.0	35.3	0.57	10.8	4.8–18.9
	H0740	10.5	1.6	16.9	0.41	14.1	4.9–19.2
	H0758	9.2	3.4	24.5	0.64	8.1	2.1–16.5
Cell with axon in all CA1 strata[b]	H0766	12.3	3.8	18.2	0.56	10.5	3.3–18.1
Cells in strata oriens or radiatum with projection to these layers, Fig. 6*B*[b]	H0368	6.7	3.3	46.4	0.37	5.1	2.2–8.5
	H0627	9.1	4.3	31.8	0.29	6.0	3.1–8.5
R-LM cells Figs 5*A*, *B*	H0637	11.1	1.1	13.4	0.34	8.7	2.1–19.6
	H0408	13.6	1.3	16.7	0.40	14.5	4.3–31.8
Pyramidal cells	H0242	7.9	5.5	35.0	0.39	8.7	2.8–13.6
	H0403	11.0	10	37.4	0.48	7.8	2.4–12.2
	H0411	10.0	1.2	27.6	0.52	9.6	1.2–15.0
Giant radiatum cell in a longitud. slice[b]	H0947	8.7	1.9	20.7	0.31	7.4	1.5–15.1

O-LM cells, Oriens/alveus interneurons projecting to str. lacunosum-moleculare; *R-LM cells*, cells in str. radiatum projecting to str. lacunosum-moleculare; *Rs*, access resistance during the period used for analysis of sIPSCs properties (2–5 min).

[a] Measured at a holding potential of 0 ± 5 mV.

[b] See Results for morphological details.

Properties of sIPSCs in oriens/alveus interneurons projecting to stratum lacunosum-moleculare (O-LM cells)

The cell bodies and dendrites of anatomically identified O-LM cells were confined to str. oriens and alveus (Fig. 1 *B*,*C*). A common morphological feature of these cells was the presence of spiny dendrites giving rise to some short branches close to their tips. In all seven cases, the main axon without varicosities originated from a proximal dendrite and crossed the pyramidal cell layer and str. radiatum. After reaching the border of strata radiatum and lacunosum-moleculare, the axon arborized almost exclusively in the str. lacunosum-moleculare where the axon collaterals became fine and varicose. Neurons with similar arborization patterns in the CA1 region have been described previously both *in vitro* and *in vivo* (McBain et al., 1994; Sik et al., 1995). Four of the seven O-LM cells had some axon collaterals in the str. oriens as well. A camera lucida reconstruction of an O-LM cell from three 80-μm-thick sections is shown in Figure 1*C*. The properties of sIPSC averages recorded in O-LM cells in coronal slices were homogeneous (Fig. 2*B*). Their average amplitude was 17.0 ± 1.5 pA, whereas the mean τ_R had a value of 0.44 ± 0.05 msec (n = 5). The distributions of amplitudes, 10–90% rise times, and T50% had similar plots in all anatomically identified O-LM cells (Fig. 2*A*; Table 1).

O-LM cells and other interneurons with a horizontal dendritic tree in the str. oriens may receive GABAergic innervation from neurons with axonal projections in a plane different from the plane of a coronal slice. Electrical stimulation experiments in the str. oriens support the possibility of such oriented projections (Lacaille and Schwartzkroin, 1988a). For example, interneuron-specific inhibitory cells immunoreactive for vasoactive intestinal polypeptide (VIP) and for the calcium-binding protein calretinin (CR) form a dense axonal plexus at the str. oriens and alveus border and may project mainly along the longitudinal axis of the hippocampus (Acsády et al., 1996a) (L. Acsády, personal communication) to innervate horizontal interneurons including O-LM cells in this layer (Acsády et al., 1996b). This anatomical finding together with the higher probability of recording spontaneous synaptic events originating from long, intact axon collaterals (Staley and Mody, 1991) would ensure a higher probability of recording O-LM cell sIPSCs in a slice cut in the longitudinal plane. Therefore, we investigated the possibility that cutting a slice along the longitudinal axis of the hippocampus may better preserve the inhibitory inputs onto O-LM cells. We obtained recordings from two additional identified O-LM cells in such a slice preparation. The overall frequency of sIPSCs in these O-LM cells was markedly higher (4.1 ± 1.2 Hz; n = 2) than that found in coronal slices (1.52 ± 0.06 Hz; n = 5; see also Table 1).

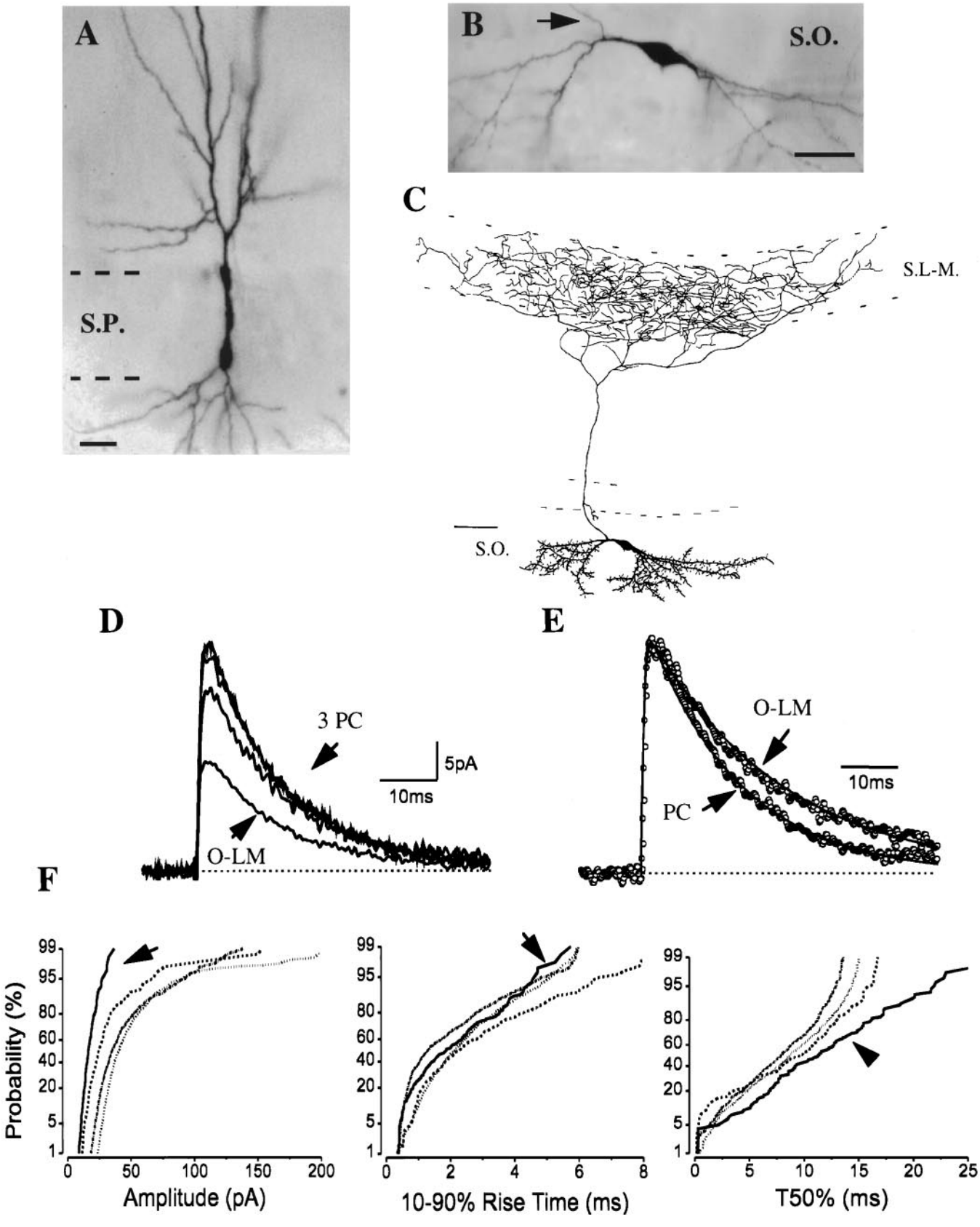

Figure 1. Comparison of sIPSC kinetics in pyramidal cells and an O-LM cell. *A*, *B*, Images of an intracellularly filled pyramidal cell (*A*; *PC*) and of an O-LM cell (*B*) were digitized after visualization of biocytin or neurobiotin (the *arrow* shows the main axon originating from a proximal dendrite). *C*, Camera lucida reconstruction of the O-LM cell in *B* from three 80-μm-thick vibratome sections. The cell had a spiny dendritic tree restricted to the str. oriens, whereas most axon collaterals were found in the str. lacunosum-moleculare. *D*, The averages of sIPSCs in three morphologically identified pyramidal cells are very similar, in contrast to the average sIPSC in the O-LM cell. *E*, The sIPSC averages (shown normalized) in a pyramidal (*Figure legend continues*)

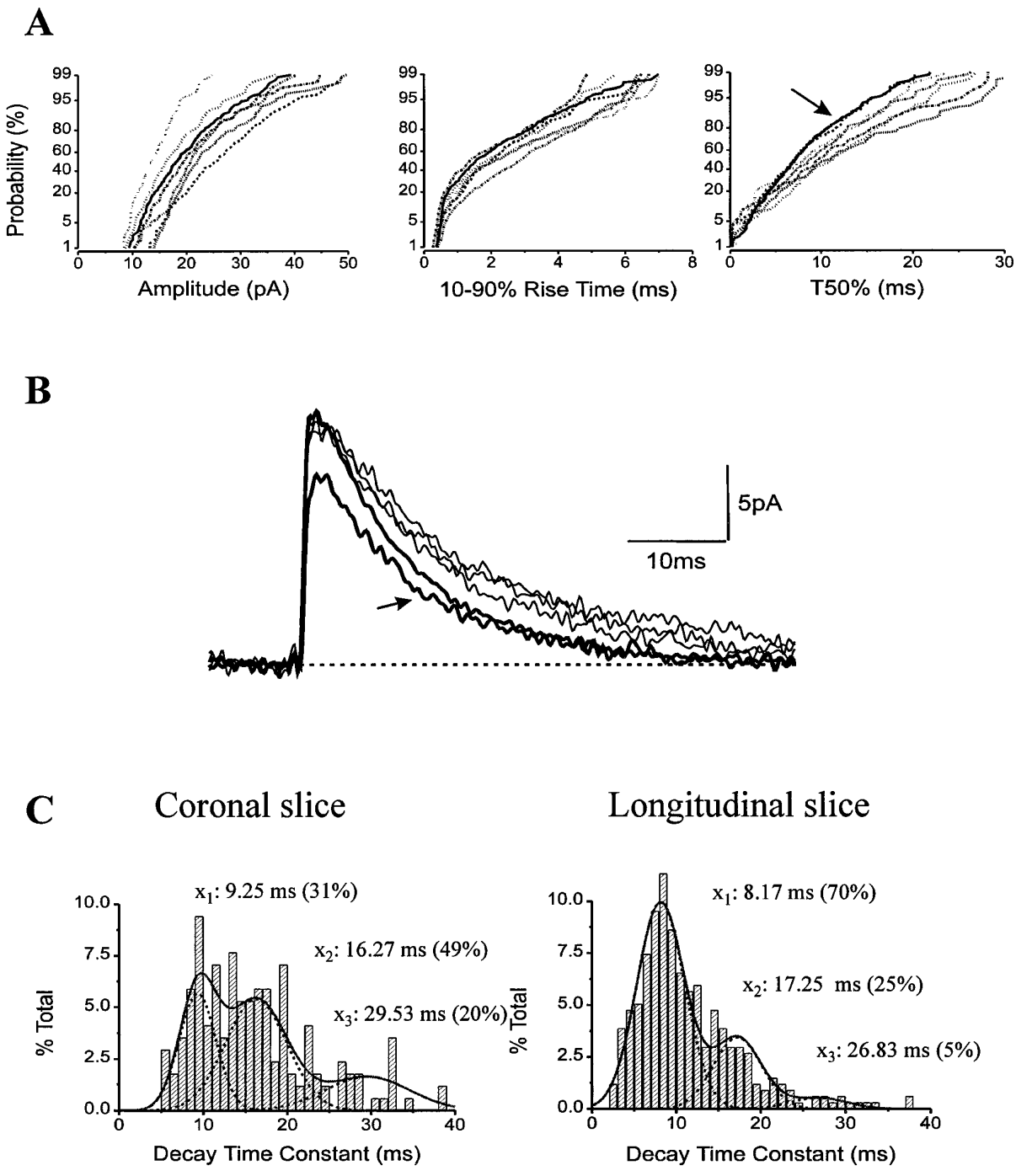

Figure 2. sIPSC kinetics in O-LM cells ($n = 5$) recorded in coronal slices were homogeneous. Accordingly, cumulative probability distributions of amplitudes, 10–90% rise times, and T50% (*A*), as well as averages (*B*, *thinner traces*), were similar among the five cells. Two additional O-LM cells sampled in longitudinal slices had matching sIPSCs (*B*, *thicker traces*; *A*, *B*, *arrows*) that differed in decay times and frequencies from sIPSCs of O-LM cells recorded in coronal slices (see Results for details). *C*, Three populations of sIPSC decay time constants denoted by the means (x_1, x_2, and x_3) were found in both coronal versus longitudinal slices. Note that the proportion of sIPSCs with fast decay time constants was considerably higher in longitudinal slices. This change caused the shift to the *left* on cumulative distributions of T50% (*A*, *arrow*) and affected the averages as well (see Table 1).

←

cell and an O-LM cell were fitted by the sum of rising and decaying exponentials (indicated by *solid line*). The fitted amplitudes of sIPSC averages markedly differed in the pyramidal cell and the O-LM cell (35.0 vs 12.2 pA), but the rise-time constants were comparable (0.39 vs 0.44 msec). The decaying phase of the average sIPSC in the O-LM cell was slower than that in the pyramidal cell. *F*, Cumulative probability plots of amplitude and T50% distributions show marked differences between pyramidal cells ($n = 3$) and an O-LM cell (*arrow*). The 10–90% rise times were not different. Kolmogorov–Smirnov (K–S) statistics indicate nonsignificant p values ($p > 10^{-4}$) for T50% among the three pyramidal cells, but the T50% distribution of the O-LM cell significantly differed from that of the pyramidal cells. Generally, pyramidal cells had sIPSCs with larger amplitudes and faster decays compared with those recorded in interneurons. Note that the cumulative distributions are comparable in all pyramidal cells. *S.O.*, Str. oriens; *S.P.*, str. pyramidale; *S.R.*, str. radiatum; *S.L-M.*, str. lacunosum-moleculare; and *S.MOL.*, str. moleculare. Scale bars: *A*, *B*, 20 μm; *C*, 100 μm.

We measured the total dendritic length of O-LM cells in both types of slices to ensure that the difference in sIPSC frequency is not a consequence of the different size of the dendritic tree spanning in coronal versus longitudinal slices. The average total dendritic lengths of O-LM cells were 1633 ± 200 μm (between 1201 and 2256 μm; $n = 5$) in coronal slices and 1683 ± 342 μm (1341 and 2025 μm; $n = 2$) in longitudinal slices. Therefore, the observed difference in frequency of sIPSCs cannot result from a significantly different dendritic morphology but rather from the different input these neurons receive in the two slice preparations. In addition to the increased frequency, the ratio of sIPSCs with fast decay time constants increased to 70% in an O-LM cell of a longitudinal slice compared with only 31% in an O-LM cell of a coronal slice (Fig. 2*C*). The other O-LM cells had similar ratios for IPSC decay time constants depending on the slice preparation. The change in the ratio of fast IPSCs is also reflected by a shift to the *left* on the cumulative probability distributions of T50% (Fig. 2*A*, *arrow*), but the amplitude and rise-time distributions were indistinguishable in the two preparations. The T50% values, but not the rise times, of sIPSCs recorded in the two O-LM cells in longitudinal slices were significantly different (K–S $p < 10^{-4}$) from the average of all O-LM cells recorded in coronal slices. In agreement with this observation, the average sIPSCs in O-LM cells from the longitudinal slices showed faster decay phases (Fig. 2*B*) but had similar amplitudes (16.9 ± 2.3 pA) and rise times (0.43 ± 0.06 msec) compared with the averages in O-LM cells of coronal slices (Table 1).

Regardless of the slice orientations, the amplitude of average sIPSCs in O-LM cells was smaller than that in pyramidal cells (Table 1). To examine the IPSC conductance in O-LM cells, we recorded sIPSCs at different holding potentials (+15, 0, −70, or −75 mV) in three identified cells (two in coronal slices and one in a longitudinal slice). The conductance was linear, and the sIPSCs reversed at E_{Cl^-} of −44.6 ± 2.6 mV ($n = 3$). The slope conductance of average sIPSC was between 0.35–0.45 nS in O-LM cells, approximately half of the conductance recorded in pyramidal cells (also see Cohen et al., 1992).

The complete anatomical identification of recorded cells helps explain the differences in sIPSC properties

Two cells located in the upper part of the str. radiatum close to str. lacunosum-moleculare showed similar small round somata and were indistinguishable by IR–DIC videomicroscopy. Moreover, after the biocytin was visualized, both cells had comparable multipolar dendritic trees at low magnification by light microscopy (Fig. 3*A*,*B*). In spite of their similar appearance, they possessed markedly different sIPSC properties (Fig. 3*F*). The cell (H0741) in Figure 3*A* had a larger average amplitude (22.0 pA) and faster decay time than did the cell (H0637) in Figure 3*B* (13.4 pA) (Fig. 3*C–E*), but their rise-time constants were similar (0.31 and 0.34 msec, respectively).

Figure 4 illustrates another example of two cells with large somata at the strata radiatum and lacunosum-moleculare border with indistinguishable appearance under IR–DIC visualization and after development of the tracer. Both cells were located close to the border of strata radiatum and lacunosum-moleculare and gave rise to several dendritic branches, including one branch toward the pyramidal cell layer. In spite of their similar morphology at low magnification in the light microscope, their sIPSC kinetics diverged considerably. A proportion of the synaptic currents from the cell in Figure 4*A* (H0408) had slow rise and decay times, as shown on the cumulative probability plots. The difference in the average sIPSCs was even more pronounced than in the previous example. Although the rise-time constants were comparable (0.40 and 0.51 msec), both the amplitudes (16.5 vs 36.6 pA) and the decay of the averages were distinct in these two cells (Fig. 4*C–E*).

Only a detailed camera lucida reconstruction of these interneurons with remarkably different sIPSC kinetics could confirm that they belonged to distinct morphological categories. The sparsely spiny dendrites of the cell in Figure 3*A* (H0741) spanned all layers of the CA1 subfield, whereas the axon ran in str. radiatum and descended into the str. oriens as well (Fig. 5*A*). In contrast, the axon of the cell in Figure 3*B* (H0637) occupied the termination zone of the entorhinal projection, i.e., mainly the str. lacunosum-moleculare, but some varicose branches also entered and ramified in the outer two-thirds of the str. moleculare in the dentate gyrus (Fig. 5*A*). Some axon collaterals were found in the str. radiatum close to the str. lacunosum-moleculare. The beaded multipolar dendritic tree of the cell bore a few spines confined to strata lacunosum-moleculare and radiatum without reaching the str. pyramidale.

The other pair of interneurons with matching somata and radial dendritic arbors but different sIPSC properties (Fig. 4*A*,*B*) had strikingly different axonal arborizations (Fig. 5*B*). Both cells gave rise to dendrites ascending to the str. lacunosum-moleculare and to descending branches toward str. pyramidale, one of them entering the str. oriens. In both cases, some spines were observed on the beaded dendritic tree. In sharp contrast to their comparable dendritic morphology, their axonal arborizations were entirely different (Fig. 5*B*). The cell in Figure 4*A* (H0408) arborized almost exclusively in str. lacunosum-moleculare without crossing the fissure. Some axon branches of this cell were also localized in the str. radiatum close to the border of str. lacunosum-moleculare. In contrast, the axon cloud of the other neuron shown in Figure 4*B* (H0414) covered all layers of the CA1 region except the str. lacunosum-moleculare (Fig. 5*B*). The majority of the axon collaterals were found in the entire str. radiatum, but a portion was also observed in both strata pyramidale and oriens.

The morphological and physiological similarities between the cells located in str. radiatum and projecting to the str. lacunosum-moleculare (R-LM cell, H0637, H0408) suggest that these cells most likely belong to a novel, yet undescribed, interneuron type in the CA1 region of the hippocampus. Some minor morphological differences were present (e.g., some axon collaterals in the str. moleculare of the dentate gyrus of the cell in Fig. 5*A*), but we will collectively refer to these interneurons as R-LM cells. In these interneurons, a considerable portion (~20%) of sIPSCs had extremely slow rise times (>10 msec), and a large fraction of sIPSCs had exceptionally slow decays, slower than those recorded in any other interneurons (see Figs. 3, 4, 8; Table 1). The other reconstructed interneurons in Figure 5*A* and *B* (H0741, H0414) may also represent the same category of nonpyramidal cells based on the comparable sIPSC kinetics and arborization patterns. Radial trilaminar cell type with comparable morphological properties has been mentioned previously without any reconstructions (Freund and Buzsáki, 1996). Therefore, in the present study we denote all interneurons in str. radiatum with ascending and descending dendrites projecting mainly to the str. radiatum and partly to strata pyramidale and oriens as radial trilaminar cells.

Recordings from three additional radial trilaminar cells, one with a similar morphology to the cell in Figure 5*A* (H0741) and two others more like the interneuron in Figure 5*B* (H0414),

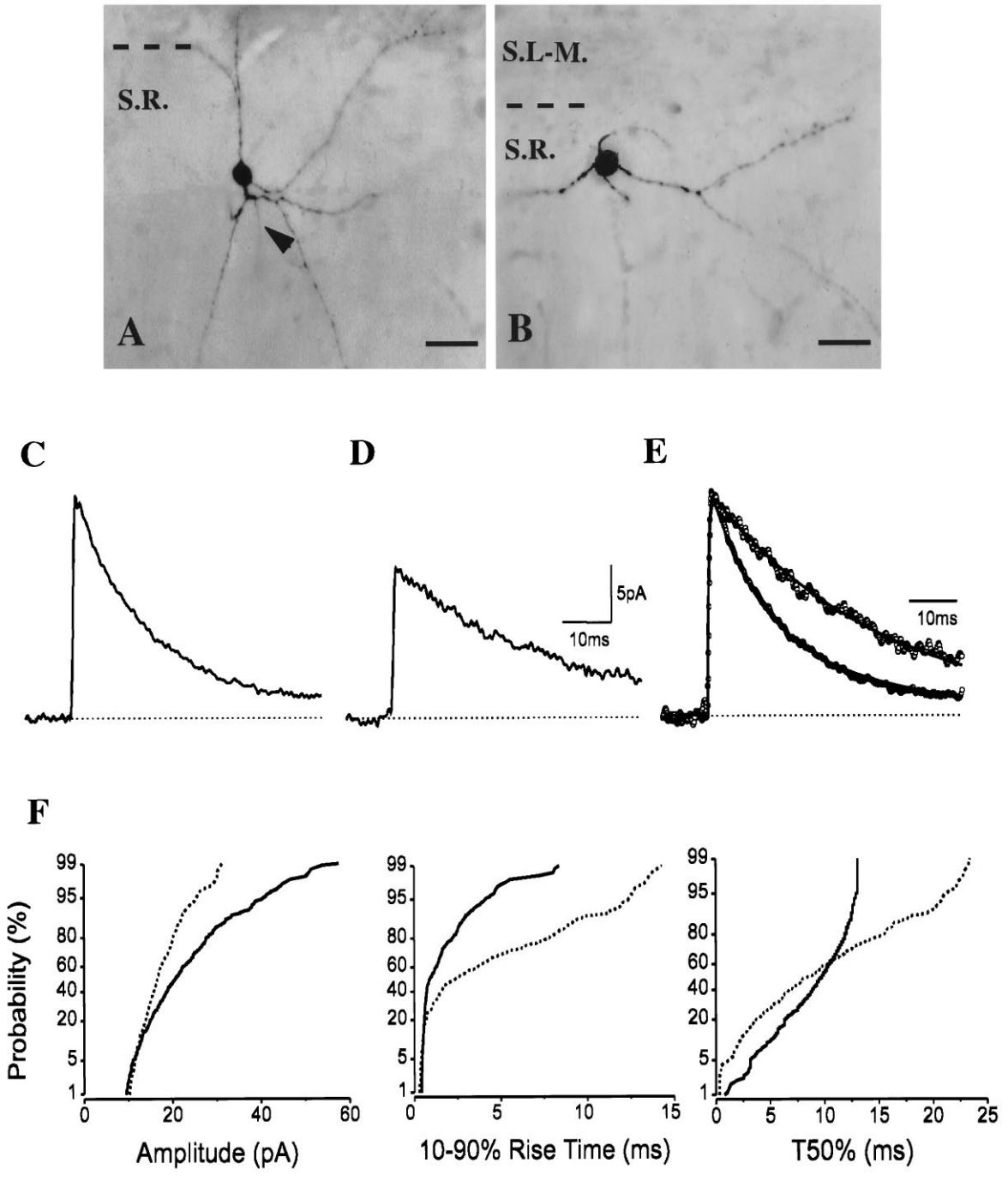

Figure 3. *A*, *B*, Images of two interneurons with similar small round cell bodies and multipolar dendritic trees in the upper part of str. radiatum (close to str. lacunosum-moleculare). The *arrowhead* in *A* marks the origin of the axon. *C*, *D*, In contrast to their matching appearance, the decaying phases of sIPSC averages showed marked differences (*C*, *D* for cells in *A*, *B*, respectively) that are more pronounced in normalized and superimposed averages (*E*). *F*, Differences in cumulative probability distributions of amplitudes, rise times, and T50% are significant (K–S $p < 10^{-4}$; *solid lines* represent the cell in *A*; *dashed lines* represent the cell in *B*). For abbreviations, see legend for Figure 1. Scale bars: *A*, *B*, 20 μm.

revealed comparable sIPSC properties as described above (see Table 1).

Comparable morphology of interneurons does not imply similar sIPSC properties

In the previous section, we have stressed the importance of a detailed anatomical distinction of interneurons to correlate with the diverse sIPSC properties. Conversely, sIPSC properties might be expected to be similar in interneurons with relatively similar morphologies. However, we have found some exceptions to this assumption. For example, Figure 6 shows two interneurons with dendritic and axonal arborization in strata radiatum and oriens in which sIPSC properties were remarkably different. A bistratified cell (Fig. 6*A*; H0759), analogous to that first reported by Buhl et al. (1994), had its cell body in str. pyramidale and gave rise to ascending and descending vertical dendrites that did not pene-

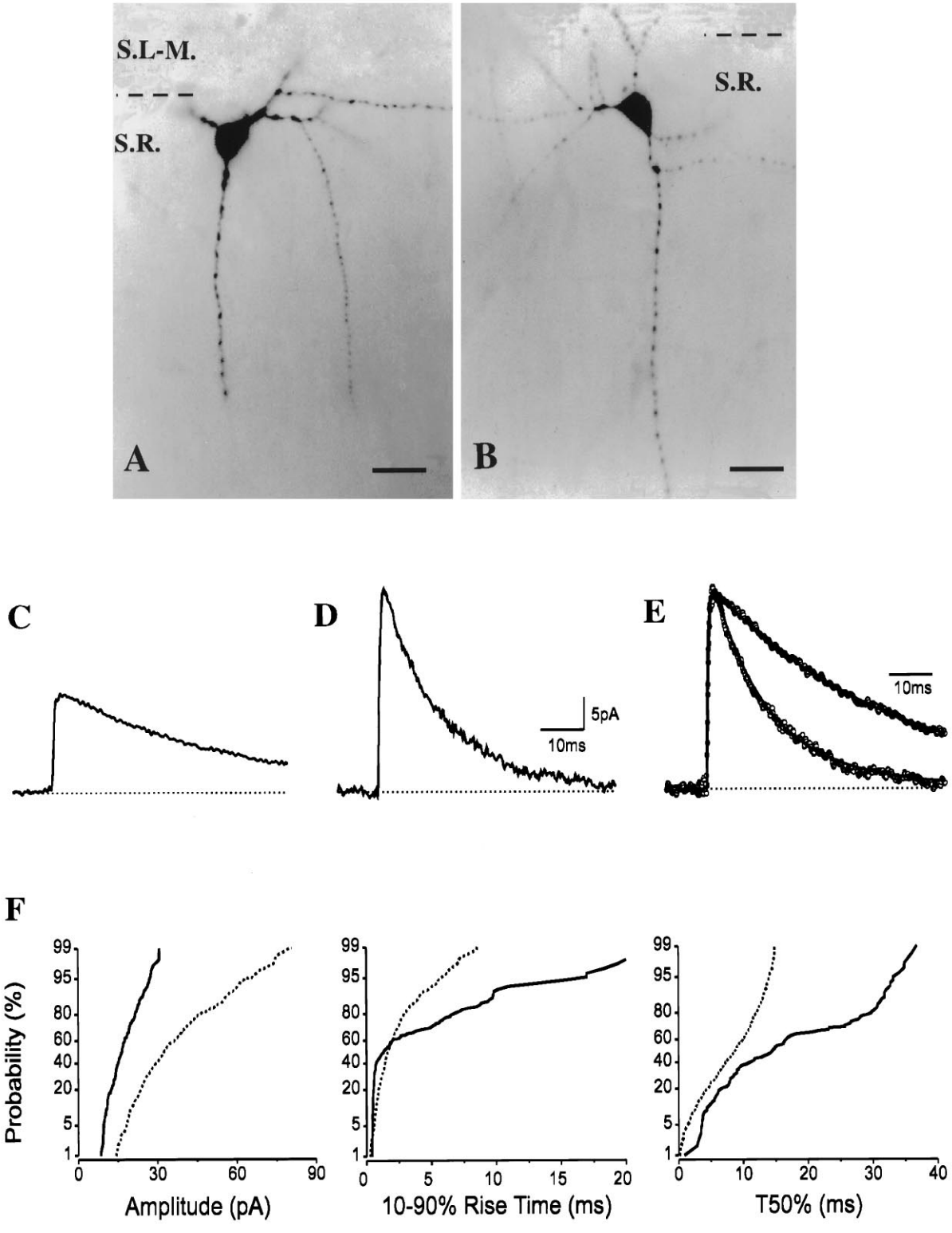

Figure 4. *A*, *B*, Images of two interneurons close to the border of strata radiatum and lacunosum-moleculare match in somata and dendritic arbors. *C*, *D*, Their average sIPSCs, however, show strikingly different decay kinetics (*C* and *D* for cells in *A* and *B*, respectively) that are more visible after superimposing the normalized *traces* (*E*). *F*, In line with this observation, the cumulative probability plots of the kinetic parameters are also significantly different (K–S $p < 10^{-4}$; *solid lines* represent the cell in *A*; *dashed lines* represent the cell in *B*). For abbreviations, see legend to Figure 1. Scale bars: *A*, *B*, 20 μm.

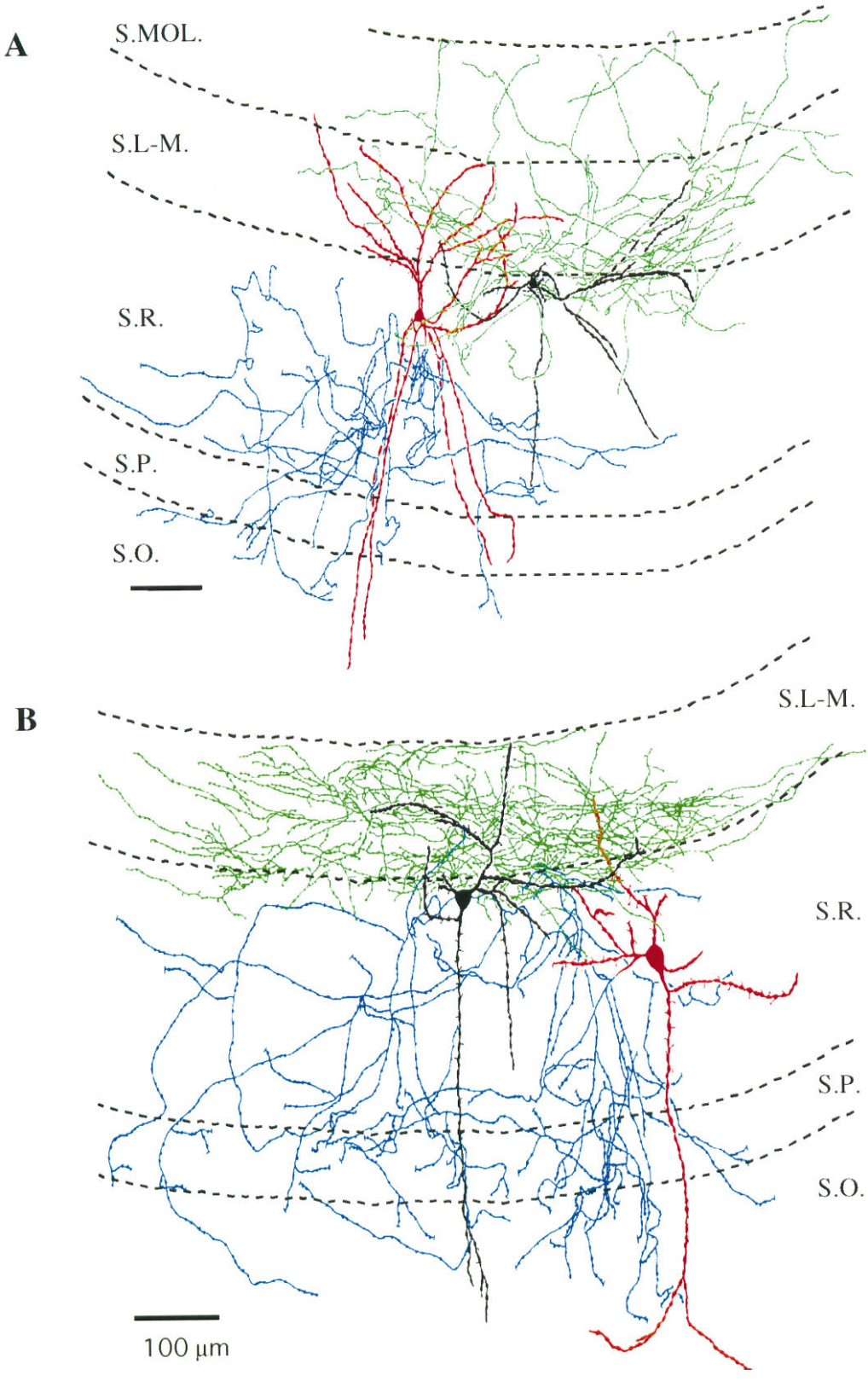

Figure 5. Camera lucida reconstructions of interneurons in Figures 3 and 4 from three to four 80-μm-thick vibratome sections. *A*, The radial trilaminar cell in Figure 3*A* gave rise to dendrites ascending and descending to all layers of the CA1 region, whereas its axon ramified mainly in str. radiatum and, after crossing the pyramidal cell layer, partly in str. oriens (dendritic arbor of the cell, *red*; axon tree, *blue*). The dendritic tree of the R-LM cell in Figure 3*B* was found to extend to strata radiatum and lacunosum-moleculare. In contrast to the radial trilaminar cell, its axonal arbor was predominantly located in conjunction with the entorhinal afferents (dendrites, *black*; axon cloud of the R-LM cell, *green*). *B*, The other R-LM cell in Figure 4*A* had dendrites spanning all strata of the CA1 region, but its axonal arbor was restricted to str. lacunosum-moleculare (dendrites, *black*; axon, *green*). In sharp contrast to the R-LM cell, the axon cloud of another radial trilaminar cell in Figure 4*B* occupied all of the layers of this subfield except the str. lacunosum-moleculare, but its dendritic tree was similar (dendrites, *red*; axon, *blue*). For abbreviations, see legend to Figure 1. Scale bars: *A*, *B*, 100 μm.

trate the str. lacunosum-moleculare. The axon cloud of the cell covered strata radiatum and oriens with only traversing collaterals in the pyramidal cell layer. The soma and the majority of dendrites of the cell depicted in Figure 6*B* (H0368) were located in str. oriens and had a rather horizontal appearance. Two dendritic branches ascended to str. radiatum, but they did not enter into the str. lacunosum-moleculare. The main axon originated from a primary dendrite, passed through the str. pyramidale, and predominantly ramified in str. radiatum. The axonal arbor was only partially reconstructed because, after curving back into the str. oriens, two main axon branches were cutoff. In summary, based on the location of their processes, both interneurons might have shared similar input and output characteristics, but they differed somewhat in their dendritic length confined to various layers.

In sharp contrast to their comparable morphology, the distributions of amplitudes, rise times, and T50% recorded in the bistratified cell and in the cell projecting to the str. radiatum (and probably to the str. oriens as well) (H0368) markedly differed (Fig. 6*F*; Table 1). In line with these data, the average sIPSCs also showed differences in amplitudes (19.1 vs 46.4 pA) and decays (Fig. 6*C–E*); however the rise-time constants were practically the same (τ_R, 0.30 vs 0.37 msec). The cell shown in Figure 6*B* (H0368) and another interneuron (H0627; Table 1) with matching rise-time and T50% distributions had the fastest-decaying average sIPSCs among all interneurons in the present study (also see Table 1). This latter cell (H0627) with fast sIPSC kinetics was found in the str. radiatum and projected to strata radiatum and oriens, but some axonal branches could be followed into the str. lacunosum-moleculare.

The properties of sIPSCs were also measured in interneurons with axonal arbors confined to the apical dendritic region of CA1 pyramidal cells. One group of cells had axon and dendritic arbors restricted to the str. radiatum (str. radiatum cells; $n = 3$). Two of the three cells had similar morphology, displaying a sparsely spiny dendritic tree (Fig. 7*A*). The other neuron (H0352; Table 1) gave rise to aspiny beaded dendrites and frequently bifurcated varicose axon collaterals similar to the cell reported by Gulyás et al. (1993). The sIPSC properties of the str. radiatum cells and their distributions were homogeneous (Fig. 7*C*,*E*,*F*; also see Table 1).

Another set of interneurons in the str. radiatum had an aspiny multipolar dendritic tree (Fig. 7*B*; $n = 3$). Several (five to seven) primary dendrites arose from the large somata and bifurcated close to their origin, giving a stellate-like appearance to these cells. The varicose axons were predominantly confined to str. radiatum, but numerous collaterals could be traced to str. lacunosum-moleculare but never crossed the fissure. Their dendritic arbors passed through all layers of the hippocampus, but the bulk of the dendrites was located in str. radiatum ($n = 2$). One such cell (H0413; Table 1) had a small round soma, and its dendrites were only confined to strata radiatum and lacunosum-moleculare. The kinetic properties of sIPSCs in these cells were homogeneous (Fig. 7*D–F*; Table 1), but their decays were faster than those recorded in str. radiatum cells (Table 1). This difference is less visible on the normalized and superimposed averages (Fig. 7*E*) but is clearly evident in the probability distribution plots of T50% (Fig. 7*F*; Table 1).

We have also recorded from an interneuron similar to that reported previously by Lacaille and Schwartzkroin (1988a) and Kunkel et al. (1988). This cell (H0766; Table 1) had a mainly horizontal dendritic tree located at the border of strata radiatum and lacunosum-moleculare, two branches descended into str. oriens. The axon emitted branches in all layers of the CA1 region (from str. lacunosum-moleculare to str. oriens), and some collaterals crossed the fissure and ramified in str. moleculare of dentate gyrus, reaching the granule cell layer as well. The sIPSCs kinetics were comparable with those recorded in radiatum cells (Table 1) with similar cumulative probability distributions (data not shown).

Table 1 summarizes the properties of sIPSCs recorded in the 28 cells of this study grouped according to their detailed anatomical identification.

Variability of sIPSCs in a given interneuron

Most sIPSCs decayed with time constants ranging between 5 and 40 msec (as long as 80 msec in the R-LM cells), showing a high degree of variability around the mean. In a given interneuron, the vast majority of individual sIPSCs (>98%) were well fitted by a single exponential decay. The multipolar cells projecting to strata radiatum and lacunosum-moleculare (Fig. 7*B*) were an exception. In all three of these cells, the fraction of events with double exponential decays was 5–8%. The variability in decay times recorded in a given cell type may result from electrotonic filtering and/or from different $GABA_A$ channel properties at different synapses. Because in CA1 interneurons rise times of synaptic events are as sensitive to electrotonic filtering as are decay times (Thurbon et al., 1994), we selected events based on their similar rise times. To avoid bias caused by different amplitudes, we selected all events over an amplitude range of 16–25 pA. The decay time constants of these selected events were plotted against the 10–90% rise times. The majority of the interneurons had plots similar to those shown for the radial trilaminar cell (H0741) in Figure 8*A*. In both cells, the 10–90% rise times could be well fitted with three Gaussian distributions (Fig. 8*A*). We chose to compare IPSCs with fast (0.2–0.9 msec) and slow (2.5–3.5 msec) rise times. Such sIPSCs selected on the basis of similar rise times could still be assigned to three groups based on their decay time constants. The decay time constants for the three groups ranged between 5 and 12 msec, 12 and 25 msec, and 25 and 45 msec. The decays of the average sIPSCs resulting from this grouping were fitted with a single exponential. In the radial trilaminar cell (H0741), sIPSCs with fast rise times could be separated into two groups with decay time constants of 10.8 and 22.4 msec, whereas the fast rise-time events in the R-LM cell (H0408) had decays of 12.3, 23.4, and 36.2 msec (Fig. 8*B*). Averages of sIPSCs with comparatively slow rise times showed the following decay time constants: 17.7 msec in radial trilaminar cell and 39.9 msec in the R-LM cell. These results indicate a large heterogeneity of spontaneous $GABA_A$ events in a given cell and among interneuron types. Although interneurons are less compact electrotonically than is suggested by their anatomy (Thurbon et al., 1994; Mott et al., 1997), the lower variance of rise times than that of decay time constants in similar amplitude events implies that distinct $GABA_A$ receptor kinetics at different synapses may contribute more importantly than electrotonic filtering to determining sIPSC diversity.

DISCUSSION

The major findings of the present study may be summarized as follows: (1) the kinetic properties of IPSCs in interneurons are different than those of pyramidal cells; (2) the characteristics of $GABA_A$ receptor-mediated synaptic transmission among interneurons show a high variability; and (3) new hippocampal CA1 interneuron types could be identified with intracellular labeling.

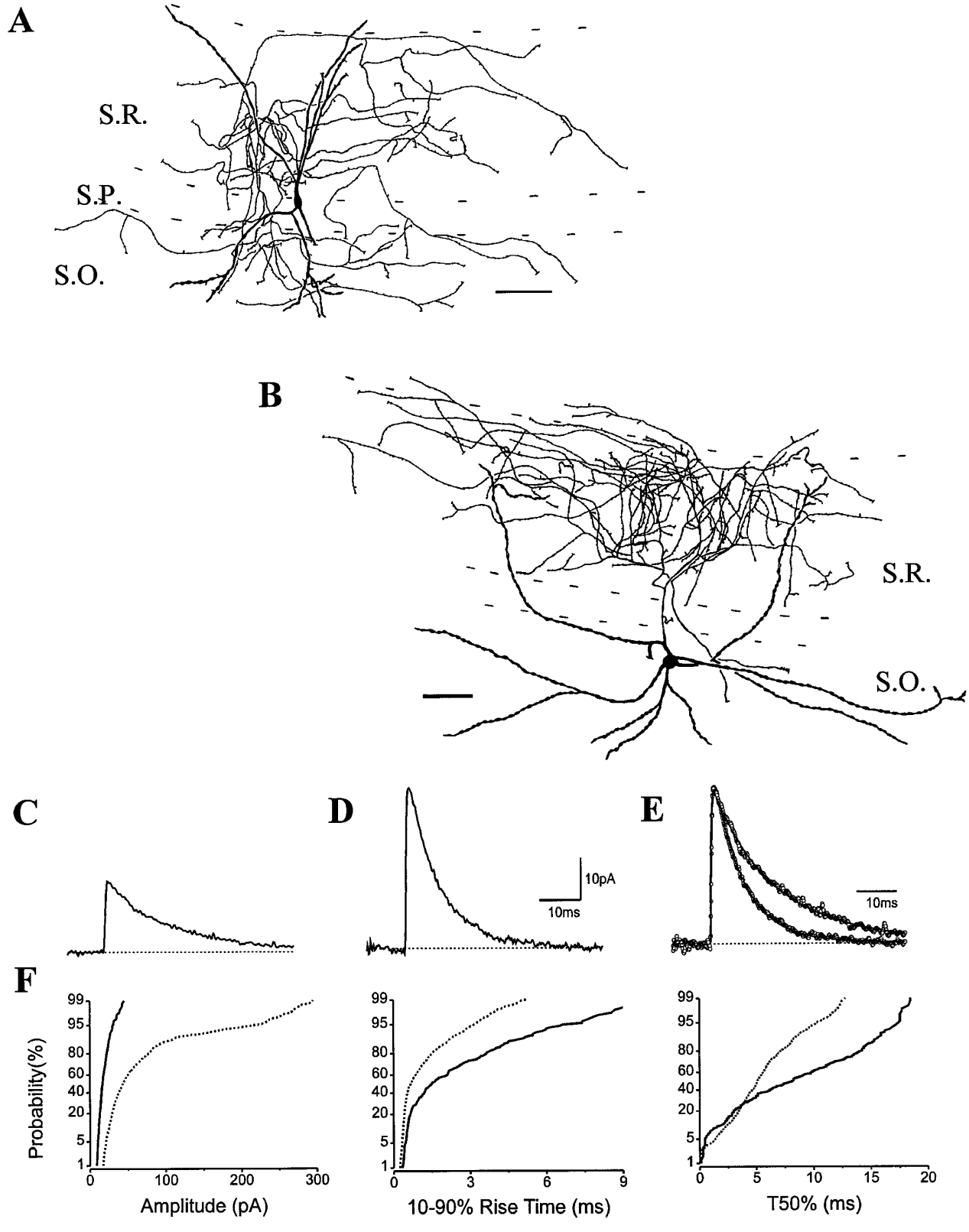

Figure 6. Interneurons with comparable morphology may show differences in their sIPSC kinetics. *A*, A bistratified cell gave rise to both axons and dendrites to strata radiatum and oriens avoiding str. lacunosum-moleculare. The main axon originated from a secondary dendrite. *B*, A cell with the soma and with the majority of the dendrites in str. oriens had axon collaterals mainly in str. radiatum, where two dendritic branches were also found. Note the two main axon collaterals left the slice in the str. oriens. (For a detailed morphological description, see Results) *C–E*, The average sIPSCs of these cells (*C* for bistratified cell and *D* for the cell in *B*) were remarkably distinct in amplitudes and decays, more visible after normalization and superimposition (*E*). *F*, The cumulative probability distributions of amplitudes, 10–90% rise times, and T50% of these interneurons differed significantly (K–S $p < 10^{-4}$; *solid lines* represent the bistratified cell; *dashed lines* represent the other cell). For abbreviations, see legend to Figure 1. Scale bars: *A*, *B*, 100 μm.

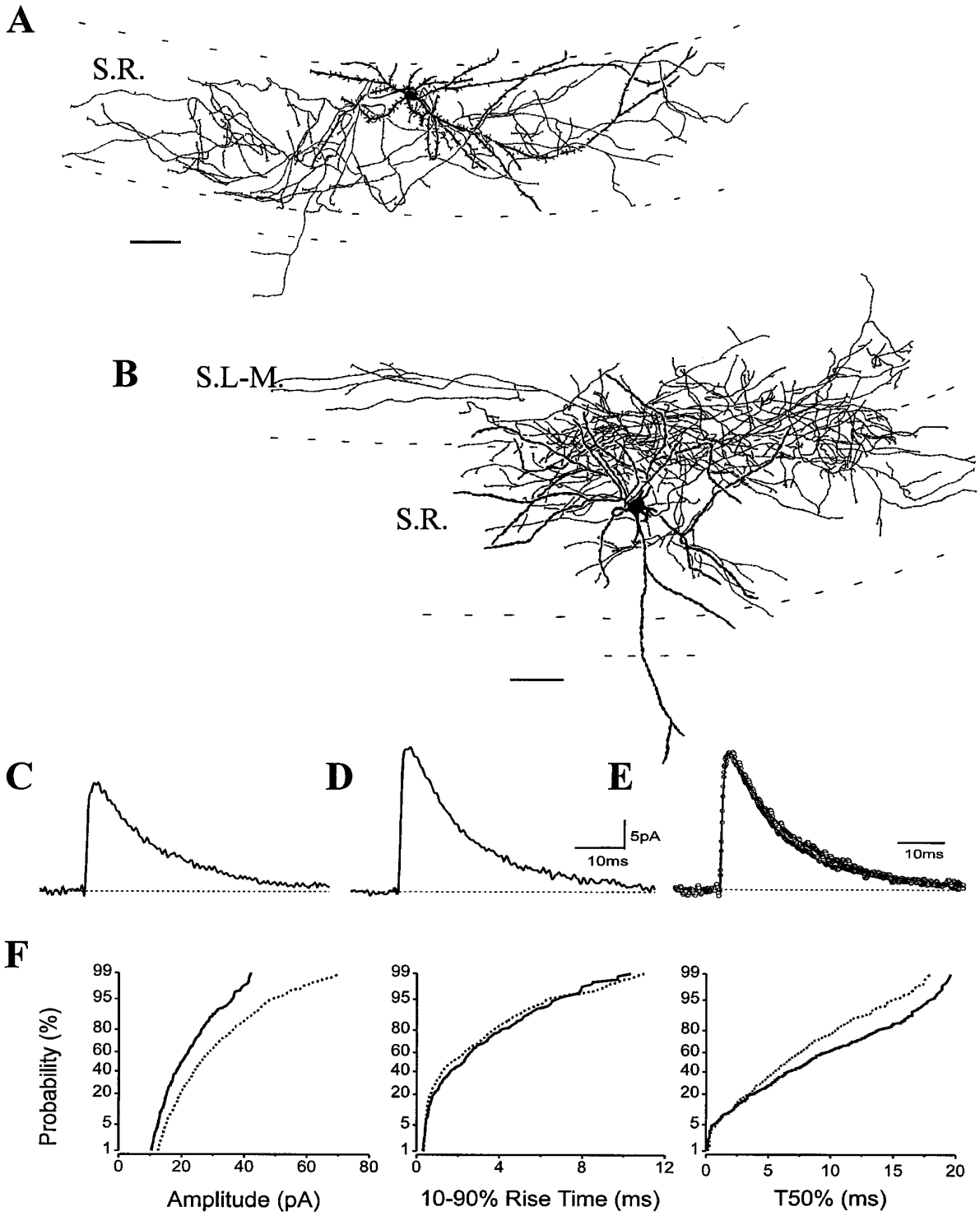

Figure 7. sIPSCs in interneurons with different morphologies. *A*, A cell in the apical dendritic region of pyramidal cells gave rise to both the axonal and dendritic branches restricted to the str. radiatum (str. radiatum cell). *B*, The dendrites and the axons of a multipolar cell with primary dendrites bifurcating close to the soma ramified mainly in str. radiatum and partly in str. lacunosum-moleculare, only one dendritic branch entered the str. oriens. The averages of sIPSCs show similar appearances (*C* for the str. radiatum cell and *D* for the multipolar cell); however after they were normalized and superimposed, the average sIPSC of the str. radiatum cell has a somewhat slower decay than that found in the multipolar cell projecting to strata radiatum and lacunosum-moleculare (*E*). *F*, This small difference in decays of the averages is more noticeable on the cumulative probability plots of T50%, although the rise times are comparable (*solid lines* represent the str. radiatum cell; *dashed lines* represent the multipolar cell). The K–S statistics indicate a nonsignificant p value of 1.2×10^{-2} for the rise time and a significant p value of $< 10^{-4}$ for the T50% distributions. Similar deviations of sIPSC decays were noticed in other identified str. radiatum cells and multipolar cells projecting to strata radiatum and lacunosum-moleculare as well (Table 1). For abbreviations, see legend to Figure 1. Scale bars: *A*, *B*, 100 μm.

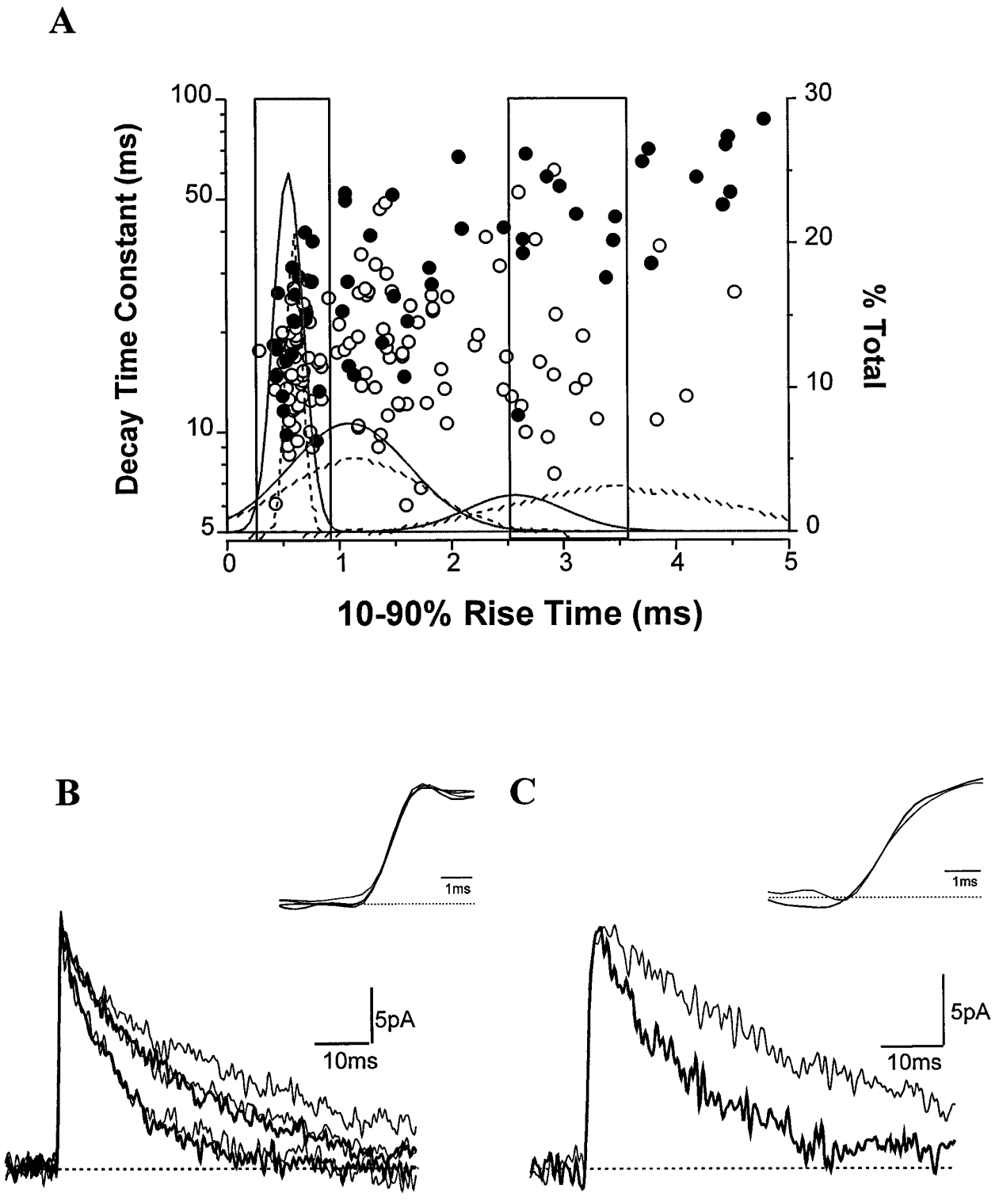

Figure 8. Rise times and decay time constants of sIPSCs in two interneurons belonging to different cell groups. *A*, The rise times of sIPSCs in the 16–25 pA amplitude range are plotted against their decay time constants (log scale). The individual events of the radial trilaminar cell (H0741) are *open circles*, whereas *solid circles* indicate sIPSCs of the R-LM cell (H0408). Note the high variability of decay time constants of sIPSCs around their averages (Figs. 3*C*, 4*C*). Also note that the events with large decay time constants are more abundant in the R-LM cell than in the radial trilaminar cell. The events in two *boxes* with fast and slow rise times were selected and averaged based on the three Gaussian distributions of the rise times (see Results for details). For the radial trilaminar cell (H0741), the trimodal distribution of the rise times (*solid line*) had the following means (± SD): 0.55 ± 0.13, 1.09 ± 0.53, and 2.57 ± 0.44 msec. The distributions for the R-LM cell (H0408) are shown with *dashed lines* and had the following means (± SD): 0.60 ± 0.07, 1.14 ± 0.62, and 3.50 ± 0.96 msec. Fast (*B*) and slow (*C*) rise-time sIPSC averages from both cells are shown superimposed. The *insets* show the rising phases at a higher time resolution. Although they had similar fast rise times, two groups of sIPSCs in the radial trilaminar cell (*thicker traces*; τ_D, 10.8 and 22.4 msec) were seen, whereas three types of decays could be seen in the R-LM cell (*thinner traces*; τ_D, 12.3, 23.4, and 36.2 msec). The decay time constants of average sIPSCs with slow rise times were 17.7 msec in the radial trilaminar cell and 39.9 msec in R-LM cells.

Kinetic properties of sIPSCs differ between pyramidal cells and interneurons

The general features of $GABA_A$ receptor-mediated spontaneous synaptic currents recorded in pyramidal cells were similar to those reported previously in pyramidal cells of the hippocampus (Collingridge et al., 1984; Cohen et al., 1992) or the neocortex (Salin and Prince, 1996). The decay time constants of sIPSCs recorded in pyramidal cells (τ_D, ~12–14 msec) differed from those recorded in dentate granule cells at room temperature (Collingridge et al., 1984; Otis and Mody, 1992; Salin and Prince, 1996). Under the same experimental conditions, the decay time constant of sIPSCs in dentate granule cells ranged between 19 and 23 msec (N. Hájos and I. Mody, unpublished observations), similar to those recorded by Otis and Mody (1992). The difference between sIPSC kinetics of the pyramidal cells and of granule cells may reflect the expression of distinct $GABA_A$ receptor subunits with different physiological properties, for example, more abundant $\alpha 5$ expression in pyramidal cells but more δ subunits in granule cells (Wisden et al., 1992).

As demonstrated for O-LM cells and pyramidal cells, the sIPSC averages and cumulative probability distributions of amplitudes, rise times, and T50% are homogeneous in a given cell type but can differ across the neuronal types. High-resolution immunocytochemistry for the $GABA_A$ receptor subunits has demonstrated the localization of $\alpha 1$, $\beta 2/3$, and $\gamma 2$ subunits in both principal cells and interneurons even at the same synapses. The main difference between the two cell groups seems to be the higher density of some $GABA_A$ receptor subunits on interneurons (Nusser et al., 1995; Somogyi et al., 1996). Our physiological data are consistent with the presence of distinct $GABA_A$ receptor subunit assemblies at various synapses on interneurons as reflected by the variety of IPSC properties.

Synaptic communication among interneurons through $GABA_A$ receptors

The $GABA_A$ receptor-mediated spontaneous synaptic currents recorded in hippocampal interneurons may originate from at least three different intrinsic and extrinsic sources: (1) from interneurons without target selectivity (for example, basket cell or str. radiatum cell; Gulyás et al., 1993; Sik et al., 1995), (2) from interneurons specifically innervating other interneurons (Acsády et al., 1996b; Gulyás et al., 1996; Hájos et al., 1996), and (3) from the GABAergic septohippocampal pathway (Freund and Antal, 1988; Tóth et al., 1997). These different inputs in a given interneuron may use different subunit combinations of $GABA_A$ receptors with distinct kinetic properties, giving an anatomical basis for this variability. This assumption is supported by our findings in O-LM cells, if interneuron-specific inhibitory cells projecting to the str. oriens/alveus border act through $GABA_A$ channels with characteristic properties that produce rapidly decaying IPSCs. The first anatomical evidence of the different localization of a $GABA_A$ receptor subunit at synapses derived from distinct hippocampal interneuron populations has been recently published (Nusser et al., 1996). In addition to the heterogeneity of the GABAergic input, the subunit expression in various hippocampal interneurons may also differ. As shown by double immunocytochemical labelings, the $\alpha 1$ subunit has been found in different subsets of neurochemically characterized interneurons (Gao and Fritschy, 1994), providing the anatomical substrate for a diversity of sIPSC kinetics among interneurons. Further research using $GABA_A$ receptor subunit selective drugs (Lüddens et al., 1995) is under way to determine the precise molecular assembly of synaptic $GABA_A$ receptors on different interneurons. The extremely slow spontaneous events with up to 40 msec decay time constants in R-LM cells may reflect distinct desensitization properties of $GABA_A$ channels in these cells. Repeated binding of GABA to the receptors at these synapses should result in a multiexponential decay kinetics (Jones and Westbrook, 1995), such as seen in a small fraction (5–8%) of sIPSCs recorded in multipolar cells projecting to the strata radiatum and lacunosum-moleculare.

Novel type of hippocampal CA1 interneurons with axonal arbors in the dendritic region of pyramidal cells

Recent *in vitro* and *in vivo* studies using intracellular labeling methods have identified several hippocampal CA1 interneuron types and have classified them according to their input and output features (Buhl et al., 1994; McBain et al., 1994; Sik et al., 1995; Freund and Buzsáki, 1996; Halasy et al., 1996; Maccaferri and McBain, 1996). Numerous physiological recordings were obtained from interneurons in this hippocampal subfield, but only two groups of dendritic inhibitory cells, namely bistratified cells and O-LM cells (Buhl et al., 1994; McBain et al., 1994; Sik et al., 1995; Halasy et al., 1996), have been morphologically characterized in detail. These cell types have been confirmed in our study as well. More recent *in vivo* studies have extended further the morphological variety to horizontal trilaminar and back-projection cells (Sik et al., 1994, 1995).

The R-LM cells in our study represent a novel interneuron type based on the characteristic sIPSC kinetics and morphological features. The presence of such cells in the CA1 region suggests that two different interneuron classes (O-LM and R-LM cells) are specialized to control the effect of entorhinal afferents on CA1 pyramidal cells with distinct input properties. The O-LM cells are likely to be excited in feedback manner, receiving their innervation mainly from local collaterals of CA1 pyramidal cells (Blasco-Ibanez and Freund, 1995; Maccaferri and McBain, 1995). In contrast, the excitatory input of R-LM cells may derive predominantly from CA3 pyramidal cells and entorhinal afferents (Ishizuka et al., 1990; Witter, 1993); thus they are likely to participate in feed-forward inhibition (Buzsáki, 1984). Their function may be to enhance the contrast between a Schaffer collateral-driven state and the entorhinal-driven state of CA1 pyramidal cells.

Interneurons with appearance similar to our str. radiatum and radial trilaminar cells have been previously alluded to, but with less complete anatomical details (Kawaguchi and Hama, 1987, 1988; Bergles et al., 1996). The multipolar cells with axon clouds in strata radiatum and lacunosum-moleculare have not been described previously, although cells with stellate-like appearance containing neuropeptide Y (NPY) and immunoreactive for substance P receptor (SPR) have been reported without any axon staining (Acsády et al., 1997). The similar dendritic morphology may mean that these multipolar cells labeled in the present study belong to the NPY and SPR-immunopositive category of interneurons.

The cells mentioned above showed similar sIPSC kinetics but displayed different morphological features. Therefore, it is not clear whether these cells represent a continuum of the dendritic inhibitory cells or whether they belong to a functionally distinct type of hippocampal interneurons.

Functional implications

According to recent modeling studies, the frequency of interneuron network oscillations should depend on the conductance and

decay time constant of $GABA_A$ receptor-mediated events (Traub et al., 1996; Wang and Buzsáki, 1996). Our recordings in a variety of interneurons show a high variability of the sIPSC decay time constants (5–80 msec) at room temperature (22–23°C). Assuming the temperature dependence of sIPSCs in interneurons is similar to that recorded in dentate granule cells (Otis and Mody, 1992), the decay time constants would vary from 2 to 30 msec at body temperature. Simulation studies of Wang and Buzsáki (1996) used connected basket cells to model an interneuron network. The critical decay time constant for generating 40 Hz oscillations was estimated to be ~10 msec (also see Traub et al., 1996). This matches the most frequently occurring sIPSC decay kinetics, between 16 and 20 msec at room temperature. Furthermore, in a morphologically identified hilar basket cell, all properties of sIPSCs (amplitude, rise time, and T50%) had very similar distributions to those found in O-LM cells or in the bistratified cell (data not shown), raising the possibility of such network activity among basket cells. In contrast to events with decay time constants in the 16–20 msec range, the fast (8–10 msec) and the much slower (30–80 msec) IPSCs at room temperature (i.e., 2–3 and 15–25 msec at 37°C) may serve as clockworks for the ultrafast (200 Hz) and theta (4–7 Hz) oscillation patterns (Buzsáki et al., 1983, 1992; Buzsáki and Chrobak, 1995; Cobb et al., 1995), respectively.

In conclusion, the high variability of sIPSCs kinetics may ensure the basis for modulating network oscillations at different frequencies. The synaptic interactions among interneurons are highly diverse but cannot be adequately resolved unless the physiological findings are always accompanied by detailed anatomical identification of the recorded interneurons.

REFERENCES

Acsády L, Arabadzisz D, Freund TF (1996a) Correlated morphological and neurochemical features identify different subsets of vasoactive intestinal polypeptide-immunoreactive interneurons in rat hippocampus. Neuroscience 73:299–315.

Acsády L, Görcs TJ, Freund TF (1996b) Different populations of vasoactive intestinal polypeptide-immunoreactive interneurons are specialized to control pyramidal cells or interneurons in the hippocampus. Neuroscience 73:317–334.

Acsády L, Katona I, Gulyás AI, Shigemoto R, Freund TF (1997) Immunostaining for substance P receptor labels GABAergic cells with distinct termination patterns in the hippocampus. J Comp Neurol 378:320–336.

Bergles DE, Doze VA, Madison DV, Smith SJ (1996) Excitatory actions of norepinephrine on multiple classes of hippocampal CA1 interneurons. J Neurosci 16:572–585.

Blasco-Ibanez JM, Freund TF (1995) Synaptic input of horizontal interneurons in stratum oriens of the hippocampal CA1 subfield: structural basis of feed-back activation. Eur J Neurosci 7:2170–2180.

Bragin A, Jandó G, Nádasdy Z, Hetke J, Wise K, Buzsáki G (1995) Gamma (40–100 Hz) oscillation in the hippocampus of the behaving rat. J Neurosci 15:47–60.

Buckmaster PS, Schwartzkroin PA (1995) Interneurons and inhibition in the dentate gyrus of the rat in vivo. J Neurosci 15:774–789.

Buhl EH, Halasy K, Somogyi P (1994) Diverse sources of hippocampal unitary inhibitory postsynaptic potentials and the number of synaptic release sites [see comments]. Nature 368:823–828.

Buzsáki G (1984) Feed-forward inhibition in the hippocampal formation. Prog Neurobiol 22:131–153.

Buzsáki G, Chrobak JJ (1995) Temporal structure in spatially organized neuronal ensembles: a role for interneuron networks. Curr Opin Neurobiol 5:504–510.

Buzsáki G, Leung L, Vanderwolf CH (1983) Cellular bases of hippocampal EEG in the behaving rat. Brain Res Rev 6:139–171.

Buzsáki G, Horváth Zs, Urioste R, Hetke J, Wise K (1992) High-frequency network oscillation in the hippocampus. Science 256:1025–1027.

Cobb SR, Buhl EH, Halasy K, Paulsen O, Somogyi P (1995) Synchronization of neuronal activity in hippocampus by individual GABAergic interneurons. Nature 378:75–78.

Cohen GA, Doze VA, Madison DV (1992) Opioid inhibition of GABA release from presynaptic terminals of rat hippocampal interneurons. Neuron 9:325–335.

Collingridge GL, Gage PW, Robertson B (1984) Inhibitory post-synaptic currents in rat hippocampal CA1 neurones. J Physiol (Lond) 356:551–564.

Freund TF, Antal M (1988) GABA-containing neurons in the septum control inhibitory interneurons in the hippocampus. Nature 336:170–173.

Freund TF, Buzsáki G (1996) Interneurons of the hippocampus. Hippocampus 6:347–470.

Gao B, Fritschy JM (1994) Selective allocation of $GABA_A$ receptors containing the α1 subunit to neurochemically distinct subpopulations of rat hippocampal interneurons. Eur J Neurosci 6:837–853.

Gray CM (1994) Synchronous oscillations in neuronal systems: mechanisms and functions. J Comput Neurosci 1:11–38.

Gulyás AI, Miles R, Hájos N, Freund TF (1993) Precision and variability in postsynaptic target selection of inhibitory cells in the hippocampal CA3 region. Eur J Neurosci 5:1729–1751.

Gulyás AI, Hájos N, Freund TF (1996) Interneurons containing calretinin are specialized to control other interneurons in the rat hippocampus. J Neurosci 16:3397–3411.

Hájos N, Acsády L, Freund TF (1996) Target selectivity and neurochemical characteristics of VIP-immunoreactive interneurons in the rat dentate gyrus. Eur J Neurosci 8:1415–1431.

Halasy K, Buhl EH, Lörinczi Z, Tamás G, Somogyi P (1996) Synaptic target selectivity and input of GABAergic basket and bistratified interneurons in the CA1 area of the rat hippocampus. Hippocampus 6:306–329.

Han ZS, Buhl EH, Lorinczi Z, Somogyi P (1993) A high degree of spatial selectivity in the axonal and dendritic domains of physiologically identified local-circuit neurons in the dentate gyrus of the rat hippocampus. Eur J Neurosci 5:395–410.

Ishizuka N, Weber J, Amaral DG (1990) Organization of intrahippocampal projections originating from CA3 pyramidal cells in the rat. J Comp Neurol 295:580–623.

Jefferys JGR, Traub RD, Whittington MA (1996) Neuronal networks for induced '40 Hz' rhythms. Trends Neurosci 19:202–208.

Jones MV, Westbrook GL (1995) Desensitized states prolong GABAA channel responses to brief agonist pulses. Neuron 15:181–191.

Kawaguchi Y, Hama K (1987) Two subtypes of non-pyramidal cells in rat hippocampal formation identified by intracellular recording and HRP injection. Brain Res 411:190–195.

Kawaguchi Y, Hama K (1988) Physiological heterogeneity of nonpyramidal cells in rat hippocampal CA1 region. Exp Brain Res 72:494–502.

Kunkel DD, Lacaille JC, Schwartzkroin PA (1988) Ultrastructure of stratum lacunosum-moleculare interneurons of hippocampal CA1 region. Synapse 2:382–394.

Lacaille JC (1991) Postsynaptic potentials mediated by excitatory and inhibitory amino acids in interneurons of stratum pyramidale of the CA1 region of rat hippocampal slices in vitro. J Neurophysiol 66:1441–1454.

Lacaille JC, Schwartzkroin PA (1988a) Stratum lacunosum-moleculare interneurons of hippocampal CA1 region. I. Intracellular response characteristics, synaptic responses, and morphology. J Neurosci 8:1400–1410.

Lacaille JC, Schwartzkroin PA (1988b) Stratum lacunosum-moleculare interneurons of hippocampal CA1 region. II. Intrasomatic and intradendritic recordings of local circuit synaptic interactions. J Neurosci 8:1411–1424.

Lacaille JC, Mueller AL, Kunkel DD, Schwartzkroin PA (1987) Local circuit interactions between oriens/alveus interneurons and CA1 pyramidal cells in hippocampal slices: electrophysiology and morphology. J Neurosci 7:1979–1993.

Llano I, Gerschenfeld HM (1993) Inhibitory synaptic currents in stellate cells of rat cerebellar slices. J Physiol (Lond) 468:177–200.

Lüddens H, Korpi ER, Seeburg PH (1995) GABAA/benzodiazepine receptor heterogeneity: neurophysiological implications. Neuropharmacology 34:245–254.

Maccaferri G, McBain CJ (1995) Passive propagation of LTD to stratum-oriens alveus inhibitory neurons modulates the temporoammonic input to the hippocampal CA1 region. Neuron 15:137–145.

Maccaferri G, McBain CJ (1996) Long-term potentiation in distinct

subtypes of hippocampal nonpyramidal neurons. J Neurosci 16:5334–5343.
McBain CJ, DiChiara TJ, Kauer JA (1994) Activation of metabotropic glutamate receptors differentially affects two classes of hippocampal interneurons and potentiates excitatory synaptic transmission. J Neurosci 14:4433–4445.
Miles R, Tóth K, Gulyás AI, Hájos N, Freund TF (1996) Differences between somatic and dendritic inhibition in the hippocampus. Neuron 16:815–823.
Misgeld U, Frotscher M (1986) Postsynaptic-GABAergic inhibition of non-pyramidal neurons in the guinea-pig hippocampus. Neuroscience 19:193–206.
Morin F, Beaulieu C, Lacaille JC (1996) Membrane properties and synaptic currents evoked in CA1 interneuron subtypes in rat hippocampal slices. J Neurophysiol 76:1–16.
Mott DD, Turner DA, Okazaki MM, Lewis DV (1997) Interneurons of the dentate-hilus border of the rat dentate gyrus: morphological and electrophysiological heterogeneity. J Neurosci 17:3990–4005.
Neher E (1992) Correction for liquid junction potentials in patch clamp experiments. Methods Enzymol 207:123–131.
Nusser Z, Roberts JD, Baude A, Richards JG, Sieghart W, Somogyi P (1995) Immunocytochemical localization of the alpha 1 and beta 2/3 subunits of the GABAA receptor in relation to specific GABAergic synapses in the dentate gyrus. Eur J Neurosci 7:630–646.
Nusser Z, Sieghart W, Benke D, Fritschy JM, Somogyi P (1996) Differential synaptic localization of two major gamma-aminobutyric acid type A receptor α subunits on hippocampal pyramidal cells. Proc Natl Acad Sci USA 93:11939–11944.
Otis TS, Mody I (1992) Modulation of decay kinetics and frequency of $GABA_A$ receptor-mediated spontaneous inhibitory postsynaptic currents in hippocampal neurons. Neuroscience 49:13–32.
Puia G, Costa E, Vicini S (1994) Functional diversity of GABA-activated Cl− currents in Purkinje versus granule neurons in rat cerebellar slices. Neuron 12:117–126.
Sakmann B, Stuart GJ (1995) Patch-pipette recordings from the soma, dendrites, and axon of neurons in brain slices. In: Single-channel recording (Sakmann B, Neher E, eds), pp 199–211. New York: Plenum.
Salin PA, Prince DA (1996) Spontaneous $GABA_A$ receptor-mediated inhibitory currents in adult rat somatosensory cortex. J Neurophysiol 75:1573–1588.
Sik A, Ylinen A, Penttonen M, Buzsáki G (1994) Inhibitory CA1–CA3–hilar region feedback in the hippocampus. Science 265:1722–1724.
Sik A, Penttonen M, Ylinen A, Buzsáki G (1995) Hippocampal CA1 interneurons: an *in vivo* intracellular labelling study. J Neurosci 15:6651–6665.
Singer W (1993) Synchronization of cortical activity and its putative role in information processing and learning. Annu Rev Physiol 55:349–374.
Soltesz I, Deschênes M (1993) Low- and high-frequency membrane potential oscillations during theta activity in CA1 and CA3 pyramidal neurons of the rat hippocampus under ketamine–xylazine anesthesia. J Neurophysiol 70:97–116.
Soltesz I, Mody I (1994) Patch-clamp recordings reveal powerful GABAergic inhibition in dentate hilar neurons. J Neurosci 14:2365–2376.
Soltesz I, Mody I (1995) Ca^{2+}-dependent plasticity of miniature inhibitory postsynaptic currents after amputation of dendrites in central neurons. J Neurophysiol 73:1763–1773.
Somogyi P, Fritschy JM, Benke D, Roberts JDB, Sieghart W (1996) The gamma2 subunit of the $GABA_A$ receptor is concentrated in synaptic junctions containing the α1 and β2/3 subunits in hippocampus, cerebellum and globus pallidus. Neuropharmacology 35:1425–1444.
Staley KJ, Mody I (1991) Integrity of perforant path fibers and the frequency of action potential independent excitatory and inhibitory synaptic events in dentate gyrus granule cells. Synapse 9:219–224.
Thurbon D, Field A, Redman S (1994) Electrotonic profiles of interneurons in stratum pyramidale of the CA1 region of rat hippocampus. J Neurophysiol 71:1948–1958.
Tóth K, Freund TF, Miles R (1997) Disinhibition of rat hippocampal pyramidal cells by GABAergic afferents from the septum. J Physiol (Lond) 500:463–474.
Traub RD, Whittington MA, Colling SB, Buzsáki G, Jefferys JGR (1996) Analysis of gamma rhythms in the rat hippocampus *in vitro* and *in vivo*. J Physiol (Lond) 493:471–484.
Vincent P, Armstrong CM, Marty A (1992) Inhibitory synaptic currents in rat cerebellar Purkinje cells: modulation by postsynaptic depolarization. J Physiol (Lond) 456:453–471.
Wang XJ, Buzsáki G (1996) Gamma oscillation by synaptic inhibition in a hippocampal interneuronal network model. J Neurosci 16:6402–6413.
Whittington MA, Traub RD, Jefferys JG (1995) Synchronized oscillations in interneuron networks driven by metabotropic glutamate receptor activation. Nature 373:612–615.
Williams S, Samulack DD, Beaulieu C, Lacaille J-C (1994) Membrane properties and synaptic responses of interneurons located near the stratum lacunosum-moleculare/radiatum border of area CA1 in whole-cell recordings from rat hippocampal slices. J Neurophysiol 71:2217–2235.
Wisden W, Laurie DJ, Monyer H, Seeburg PH (1992) The distribution of 13 $GABA_A$ receptor subunit mRNAs in the rat brain. I. Telencephalon, diencephalon, mesencephalon. J Neurosci 12:1040–1062.
Witter MP (1993) Organization of the entorhinal–hippocampal system: a review of current anatomical data. Hippocampus 3:33–44.